New Journal of Physics
The open access journal at the forefront of physics

Deutsche Physikalische Gesellschaft DPG IOP Institute of Physics

PAPER • OPEN ACCESS

Nanoscale patterning, macroscopic reconstruction, and enhanced surface stress by organic adsorption on vicinal surfaces

To cite this article: Florian Pollinger *et al* 2017 *New J. Phys.* **19** 013019

IOP Publishing New J. Phys. 19 (2017) 013019 doi:10.1088/1367 2630/aa55b8

New Journal of Physics
The open access journal at the forefront of physics

Deutsche Physikalische Gesellschaft DPG
IOP Institute of Physics

Published in partnership with: Deutsche Physikalische Gesellschaft and the Institute of Physics

OPEN ACCESS

RECEIVED
14 September 2016

REVISED
21 December 2016

ACCEPTED FOR PUBLICATION
23 December 2016

PUBLISHED
16 January 2017

PAPER

Nanoscale patterning, macroscopic reconstruction, and enhanced surface stress by organic adsorption on vicinal surfaces

Florian Pollinger[1,4], Stefan Schmitt[1], Dirk Sander[2], Zhen Tian[2], Jürgen Kirschner[2], Pavo Vrdoljak[1], Christoph Stadler[1], Florian Maier[1], Helder Marchetto[3], Thomas Schmidt[3], Achim Schöll[1,5] and Eberhard Umbach[1]

[1] University of Würzburg, Experimental Physics VII, Am Hubland, D 97074 Würzburg, Germany
[2] Max Planck Institute for Microstructure Physics, Weinberg 2, D 06120 Halle, Germany
[3] Fritz Haber Institute of the Max Planck Society, Chemical Physics, D 14195 Berlin, Germany
[4] Present address: Physikalisch Technische Bundesanstalt (PTB), Bundesallee 100, D 38116 Braunschweig, Germany.
[5] Author to whom any correspondence should be addressed.

E mail: achim.schoell@physik.uni wuerzburg.de

Keywords: patterning, reconstruction, surface stress, STM, SPA LEED, vicinal surfaces, adsorprion

Supplementary material for this article is available online

Abstract

Self-organization is a promising method within the framework of bottom-up architectures to generate nanostructures in an efficient way. The present work demonstrates that self-organization on the length scale of a few to several tens of nanometers can be achieved by a proper combination of a large (organic) molecule and a vicinal metal surface if the local bonding of the molecule on steps is significantly stronger than that on low-index surfaces. In this case thermal annealing may lead to large mass transport of the subjacent substrate atoms such that nanometer-wide and micrometer-long molecular stripes or other patterns are being formed on high-index planes. The formation of these patterns can be controlled by the initial surface orientation and adsorbate coverage. The patterns arrange self-organized in regular arrays by repulsive mechanical interactions over long distances accompanied by a significant enhancement of surface stress. We demonstrate this effect using the planar organic molecule PTCDA as adsorbate and Ag(10 8 7) and Ag(775) surfaces as substrate. The patterns are directly observed by STM, the formation of vicinal surfaces is monitored by high-resolution electron diffraction, the microscopic surface morphology changes are followed by spectro-microscopy, and the macroscopic changes of surface stress are measured by a cantilever bending method. The *in situ* combination of these complementary techniques provides compelling evidence for elastic interaction and a significant stress contribution to long-range order and nanopattern formation.

It is well established that the formation of interfaces, e.g. by adsorption of atoms or small molecules on a metal or semiconductor surface, can lead to (changes of) reconstructions of the surface on atomic scales and hence to new geometric and electronic interface structures [1]. In some cases it has been argued that such reconstructions lead to regular nanoscopic patterns, which may be used to align molecules [2–5] or as templates for the subsequent buildup of three-dimensional (3D) nanostructures [6–10]. It is less well established, however, that such reconstructions can occur on large (mesoscopic) scales [11–14]. And it is hardly known that such reconstructions involving considerable mass transport of several substrate layers can even be induced by adsorption of large organic molecules, which are also used in organic devices.

In the present work we present experimental evidence for this phenomenon. Several complementary *in situ* methods are employed to investigate the possible changes as function of preparation parameters and to understand the underlying mechanisms for microscopic and mesoscopic reconstructions. It is particularly shown that the adsorption of a large organic molecule on vicinal metal surfaces can lead to very significant

(measurable) changes of the surface stress which—together with differences of the molecular bonding on different faces—is the origin of the formation of large-scale reconstructions of the interface.

The present finding has several implications. For example, the resulting regular and tunable surface patterns can be utilized as templates for the bottom-up fabrication of 3D nanostructures. Moreover, it may help to understand mechanisms that may lead to failure of multilayer devices, for instance organic light emitting devices or organic field effect transistors, under operating conditions, because—as described here - the attractive forces of large organic molecules and elevated temperatures may lead to huge mass transport at the interfaces of metal contacts causing short-circuits or changes of the interface properties. And the observations are interesting as such since they lead to a deeper understanding of the subtle interplay between microscopic bonding differences and large scale reconstructions involving elastic interactions on the mesoscale.

As present example we have chosen the archetype system PTCDA on Ag surfaces. PTCDA (3, 4, 9, 10-perylene tetracarboxylic acid dianhydride) is a planar heterocyclic molecule with D_{2h} symmetry. It has been used as model system in many surface studies, but it has also been integrated as p-type transport layers in organic LEDs [15] and FETs [16, 17]. The first PTCDA monolayer forms a commensurate superstructure on Ag(111) [18–20]. The matching geometric parameters of the [102] plane of PTCDA single crystals in the β-modification and those of the Ag(111) plane allow epitaxial growth of PTCDA multilayers under certain, well-defined preparation conditions [21–24]. In previous studies [25, 26] we have investigated adsorption on vicinal Ag surfaces with high step densities, i.e. surfaces the normal of which is a few degrees off the [111] direction. The resulting occurrence of step bunching and large-scale reconstructions which are accompanied by pronounced changes of the global surface stress are the topic of the present paper.

Figure 1 shows STM images of the resulting Ag surface morphology after PTCDA adsorption on two different kinds of stepped Ag surfaces (sketches of these surfaces are displayed in figure S2 of the supporting information). Before deposition, the Ag(775) and Ag(10 8 7) surfaces had carefully been cleaned by ion-bombardment and annealing, and they showed no impurities in photoemission spectra. This preparation resulted in LEED patterns characteristic for Ag(111) with superimposed spots representative for the occurrence of sequences of equally spaced monoatomic steps and atomically flat (111) terraces in between. The STM images of the clean Ag surfaces confirm that the selected angle of inclination of 8.5° of the (global) surface normal with respect to the [111] direction had led to equally spaced monoatomic steps between (111) terraces of about 1.6 nm. The almost constant terrace width is ascribed to repulsive elastic interactions between the steps [25]. The STM image of figure 1(a) had been taken after deposition of 0.3 ML (1 ML defines a saturated monolayer) PTCDA onto Ag(775) at 200 K and annealing at 350 K. The STM image reveals a pattern of linear stripes consisting of PTCDA monolayers on high-index faces ('step bunches'), separated by uncovered Ag(111) terraces. This reorganization of the surface is caused by the relatively strong interaction of PTCDA with Ag atoms and has been described and discussed in detail previously [25].

Also on the Ag(10 8 7) surface (figure 1(b)) patterns of covered PTCDA areas on high-index faces are found [25] but in this case—after deposition of 0.4 ML—the (rhombic) pattern is more complicated. The reason is that the tilt angle of the global (10 8 7) surface orientation with respect to the low index direction (111) is azimuthally rotated such that the monoatomic steps have many kinks. This differs from the (775) surface which was chosen such that the steps are straight (ideally without kinks). The high kink density of the (10 8 7) surface resulted in the occurrence of different types of covered high-index faces, which form according to their thermo-dynamically favored composition upon PTCDA deposition and annealing.

The microscopic process that leads to the formation of these regular patterns has been studied in detail and has been described in a previous publication [25]. Briefly, deposition of few PTCDA molecules onto the clean (stepped) surfaces leads to preferential adsorption of the first molecules on double steps which are pulled together by the adsorption bond. The latter is apparently stronger on a double step as compared to that on the low-index (111) plane, and this stronger interaction over-compensates the repulsive interaction between adsorbate-free steps. Thus stripes of adsorbed molecules on top of double steps are formed, and further molecules are attached to these stripes by attracting further steps thus forming step bundles. These PTCDA-covered step bundles develop and grow in width with increasing PTCDA coverage and availability of 'free' steps until all steps are bundled and covered [25]. Since the step bundles form ordered arrays they become facets and new vicinal surfaces, respectively [25]. A documentation and assignment of all observed facets is given in [25] and in the supporting information. The multitude of observed superstructures will be discussed in an upcoming publication.

This happens, for instance, at 0.4 ML for the Ag(10 8 7) surface. In this case, the 'step bundles' have developed into vicinal surfaces, which are better described as new faces (or facets) by their Miller indices as indicated in figure 1(b). Now the bundling preferentially leads to a splitting of the initial step direction [1–32] into two new step directions [1–54] and [1–21] which belong to (954) and (321) facets, respectively. The new steps have significantly less kinks ([1–54] orientation for the (954) facets) or a zigzag structure ([1–21] orientation for the (321) facets) which—due to their symmetry—probably provide 'better' adsorption sites for

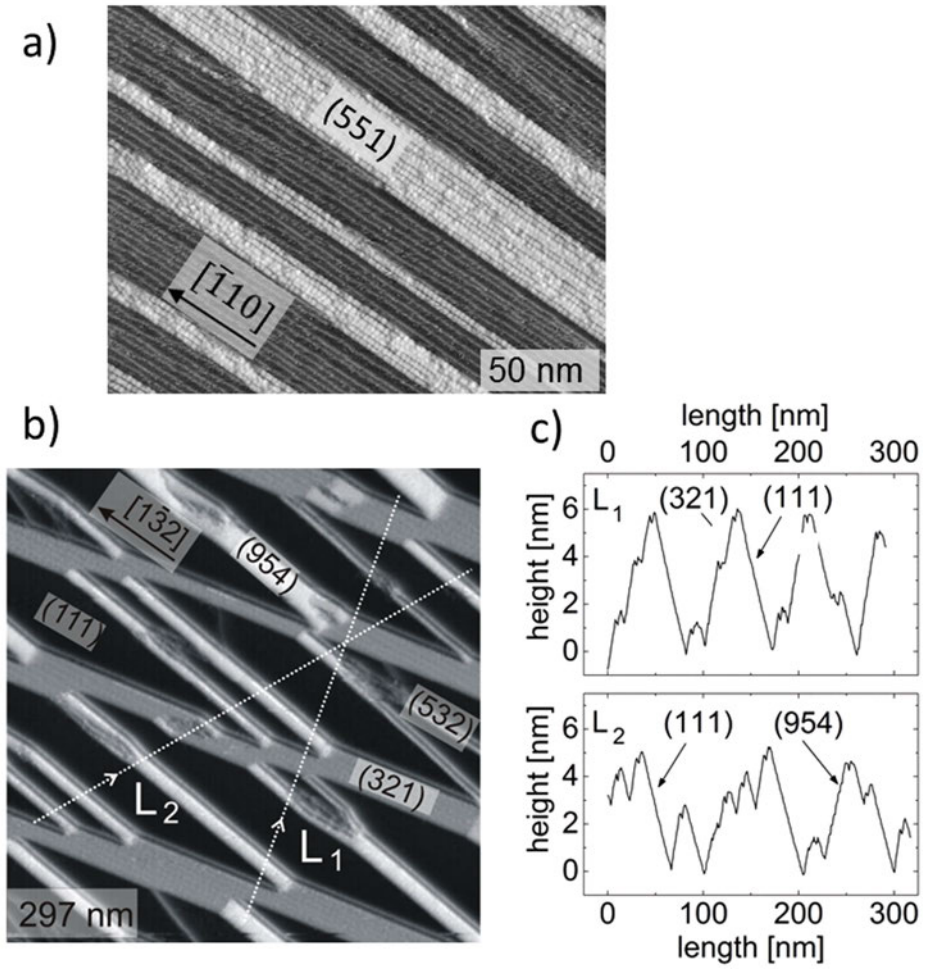

Figure 1. (a) STM images of 0.3 ML PTCDA adsorbed on a Ag(775) substrate at 200 K and annealed at 350 K; the step direction [110] and the predominant facet (551) are indicated. (b) 0.4 ML PTCDA on Ag(10 8 7) deposited at 550 K; the three different facet types ((111), (321), and (954)) present in the depicted region of (b) are labeled, and the pristine step direction [1 32] and one remnant (532) facet are indicated. The field of view of the images (a) and (b) is 50 nm and 297 nm, respectively. The labeling of the facets was derived from a careful analysis of STM and LEED data using energy dependent reciprocal space maps for the latter [25]. More details like tilt angles and superstructure data can be found in [25, 26]. (c) Line scans recorded along the dotted lines L1 (top) L2 (bottom) in (b). The survey scans (a) and (b) were taken in derivative imaging; the Ag(111) terraces appear dark. The line scans were deduced from a separate topographic scan at the locations L1 and L2 indicated in figure 1(b). The scan directions are indicated by the arrows in (b).

PTCDA adsorption and hence lead to a lower overall free energy. The two vicinal faces, (954) and (321), apparently counterbalance each other in view of their deviation from the (111) orientation in order to keep the global orientation (10 8 7) and the original (global) step direction [1–32]. The line scans in figure 1(c) show that the height differences of the regular surface structures are considerable (6 nm) on a length scale of about 100 nm, and that the mentioned vicinal faces prevail. We emphasize that in particular this figure shows that an enormous mass transport of Ag atoms has taken place, as the surface developed from a smooth clean Ag surface with equally-spaced single-atomic steps to a partly PTCDA-covered surface with a regular corrugation of 6 nm amplitude on a length scale of 100 nm. What is the reason for such a strong, large-scale surface restructuring?

In a previous publication [25] we have given an explanation for this selective behavior. Briefly, adsorption and annealing cause the surface to approach its thermodynamically most stable state, i.e. to minimize the (projected) surface free energy. The bonding of PTCDA to vicinal faces is apparently considerably stronger than to the (111) surface and stronger than the repulsive interaction between steps. Thus step bundling occurs until—for a certain coverage-PTCDA-covered vicinal faces between uncovered (111) faces are formed. The question why certain faces with steps that have reduced kink densities are preferred can be tentatively explained by differences in the bonding strength and long-range ordering (i.e. differences in the packing density) leading to a gain of surface free energy for certain faces as compared to others [25]. Both arguments are supported by previous results showing that the electronic valence structure is rather different for different surface orientations [19, 27], and that the highly ordered adsorbate layers of PTCDA on various vicinal surfaces have rather different superstructures [20, 28].

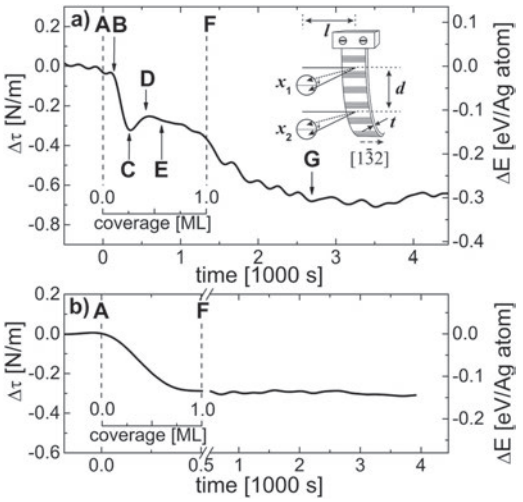

Figure 2. Surface stress change $\Delta\tau$ during adsorption of 1 ML of PTCDA on silver surfaces at 550 K. The data have been smoothed. Start and end of the PTCDA exposure are indicated by dashed lines (labeled A and F) and converted into coverage displayed by the additional scale. (a) PTCDA/Ag(111). (b) PTCDA/Ag(10 8 7). Characteristic points are marked by capital letters B E and G. The inset illustrates the two beam optical reflection technique and indicates the macroscopic orientation of the pristine step direction [1 32]. Relevant quantities for the determination of stress change are indicated (thickness of cantilever t, distance between sample and diode l, distance between two probing spots d, two respective deflections x_1 and x_2; see supplement for more details). The scaling of the horizontal axis has been adjusted to ease the comparison of the exposure intervals A F.

The question that remains to be answered, however, is why do regular patterns of PTCDA covered vicinal faces develop? Of course, one can speculate that repulsive forces between these vicinal faces are the origin, but these must be long-range mechanical forces because electronic interactions decay due to Thomas-Fermi screening on a length scale of a few nm, while the length scales of the adsorbate-induced pattern formation here are of the order of 100 nm. Moreover, if such mechanical forces contribute to the pattern formation, they should be measurable with a suited technique, such as the cantilever bending technique [29, 30].

Such cantilever bending experiments have been performed utilizing two 0.15 mm thin Ag single crystals ((10 8 7)- and (111)-oriented) that have been cleaned in UHV (see supplement). Figure 2 shows the PTCDA-induced surface stress changes $\Delta\tau$ during exposure of 1 ML PTCDA at 550 K. In order to link the surface stress $\Delta\tau$ to the respective microscopic quantity, this value is converted to an effective energy change ΔE (right axis) by multiplication with the average surface area per silver atom (7.23 Å^2).

The data show that the adsorption of one monolayer of PTCDA on both substrates causes a compressive (negative) surface stress change $\Delta\tau$ of (-0.30 ± 0.05) N m^{-1} and (-0.67 ± 0.10) N m^{-1} for the (111)- and (10 8 7)-orientation, respectively. Note that the stress change of the faceting (10 8 7) surface is more than twice that of the non-faceting (111) surface. In the case of the latter sample, $\Delta\tau$ resembles in its monotonic decrease with increasing adsorbate coverage (compare figure 2(a)) the behavior of systems characterized by a chemisorptive bonding [30], in agreement with our spectroscopic results [27, 31]. In contrast to this monotonic decrease, figure 2(b) shows that the formation of a faceted interface is associated with a complex coverage dependence of the surface stress change with regimes of constant or even tensile (positive) stress changes during exposure to the molecules. Moreover, in this case the surface stress continues changing even after exposure to PTCDA has been stopped by closing the shutter of the evaporator. A steady surface stress is reached after some 1500 s, and this indicates the timescale of the dynamic surface restructuring.

We assign this non-trivial stress behavior to different stages of the evolution of the system morphology. To scrutinize this interpretation and to learn more about the different stages of surface development, the transition was studied by two further complementary methods, SPA-LEED and LEEM which are sensitive to structural changes. (10 8 7)-oriented 1 mm thick silver crystals were used as substrates for these experiments. We emphasize that the LEED patterns proved identical faceting for the equivalent (but physically different) samples used in the different experiments (see supplement S1). Dark field LEEM experiments [32] revealed the structural changes in real space. Three major changes can be identified in figure 3 which displays three characteristic snapshots of a faceting transition. The field-of-view of the sample was chosen such that different morphologies, including areas with a high density of step bunches, were probed. According to the data depicted in figure 3, the molecules first nucleate on areas of very high step density (dark areas in figure 3(a)) as indicated by a local change of LEEM contrast (corresponding to the phase between points A and B in figure 2(b)). During this phase, submicron PTCDA domains evolved with multiple orientations, as confirmed by local LEED measurements and in agreement with the results of a detailed LEEM investigation [33].

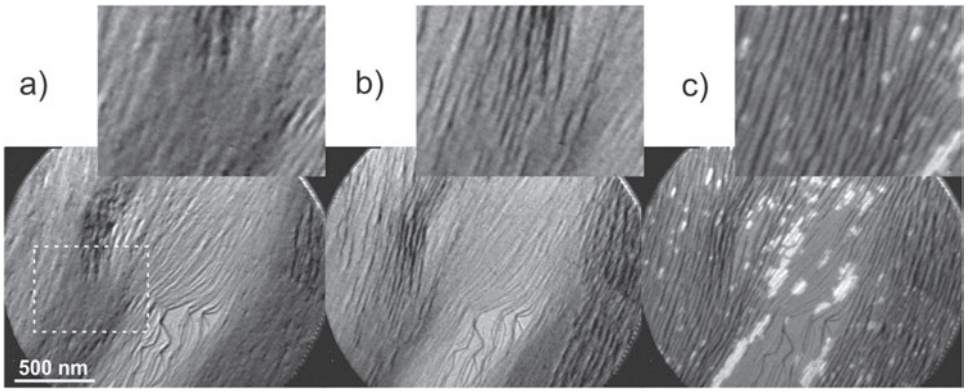

Figure 3. Major stages in the faceting transition of the Ag(10 8 7) surface during PTCDA adsorption as observed by dark field LEEM at (a) 0.07 ML, (b) 0.20 ML and (c) 0.56 ML, corresponding to the characteristic phases A B, B D and D F identified in the stress change diagram (figure 2(a)). The blow ups are the magnifications of the dashed lined area in (a). The imaging conditions are chosen such that (111) terraces appear brighter, while high index facets and steps appear dark. Islands of ordered PTCDA/Ag(111) superstructures appear white [34].

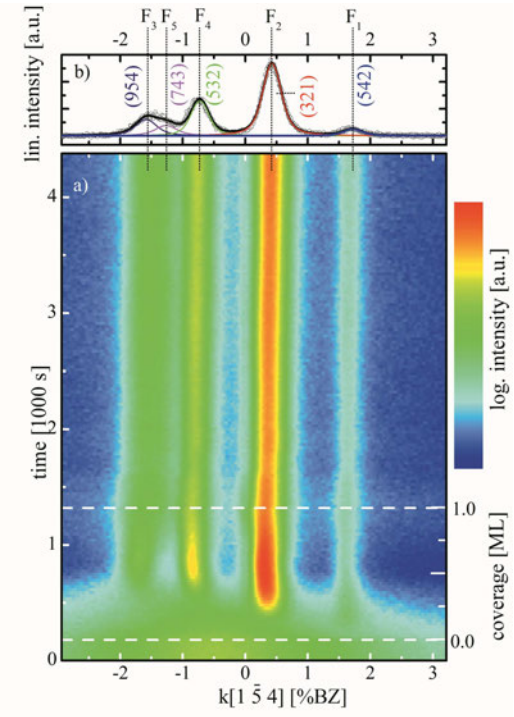

Figure 4. (a) Growth of facets during adsorption as monitored by SPA LEED. The image consists of 165 consecutive line scans. The PTCDA exposure time is indicated by dashed lines and converted into coverage by the scale on the right side. (b) Fit assuming five different facet types applied to the last line scan of figure 4(a).

Between points B and D (figure 2(b)), new facets develop on the large areas which have the average orientation of the global surface (see figure 3(b)). These facets appear as 'ripples' in the blown-up insets. In the last phase of the exposure (between D and F in figure 2(b)), the (111) terraces become covered, forming the well-known PTCDA superstructure [20] (compare bright areas in figure 3(c)). Note that the PTCDA molecules diffuse over very large distances (several tens of microns at 550 K) before they become chemisorbed on their final adsorption sites [23, 34].

Additional information on the crystallography of the facets could be gained by *in situ* high-resolution (spot profile analysis) low energy electron diffraction (SPA-LEED) [35, 36]. A spot profile of this integral technique is displayed in figure 4(b)). It represents an intensity scan along one direction in reciprocal space that contains superstructure spots from prominent vicinal faces as indicated. Such spot profiles recorded as function of coverage are plotted against time/coverage in figure 4(a). The resulting pseudo 3D graph displays intensity variations of some spot profiles and reveals changing contributions of the various vicinal faces as function of

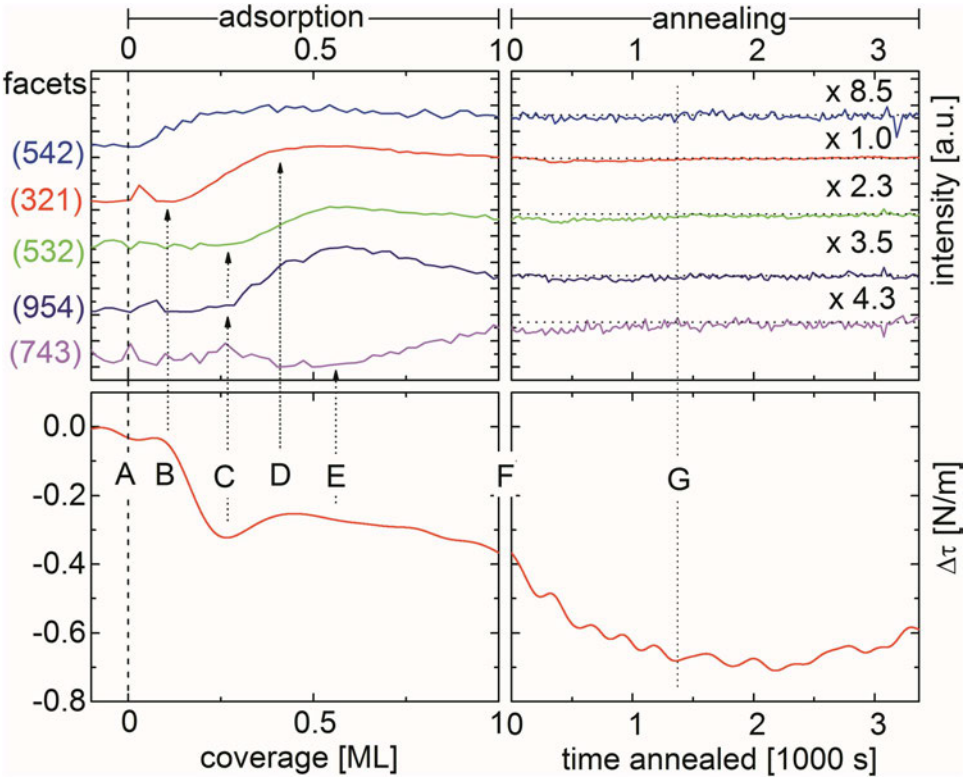

Figure 5. Correlation of the quantitative SPA LEED (top) and surface stress change (bottom) data during PTCDA adsorption (left side) and prolonged annealing (right side), both at 550 K. The SPA LEED intensity data is depicted for each facet type separately. Their asymptotic intensities after prolonged annealing are indicated by dotted horizontal lines. Vertical dotted lines and arrows indicate the correlation between characteristic changes of surface stress and facet formation. The labels A G are chosen according to figure 2. Note that two faces, (532) and (954), grow simultaneously starting at point C.

coverage. The broad intensity background at the beginning (bottom of figure 4(a)) resulted from diffuse scattering at the tail of the (00) spot of the (10 8 7) surface.

Five features (F_1–F_5) could be distinguished as function of PTCDA coverage which are assigned to the specular reflections from the facets indicated in figure 4(a). In order to map the dynamics of the faceting, the line scans were fitted consistently by five peaks according to the example presented in figure 4(b). Voigt profiles with fixed Gaussian widths provided an optimal description of the peak shapes after a linear background had been subtracted. The thus derived intensities are compared to the surface stress curve in figure 5 to correlate the facet formation (top panel) with the surface stress change (lower panel). The comparison demonstrates that every change of the curvature of the $\Delta\tau$ curve coincides with a new stage in the morphologic transition.

At very low coverage a number of differently oriented micro-facets are formed preferably in defect areas (see also LEEM data). The stress fields of these initial facets do not add up constructively to a mesoscopic strain field. Therefore, the surface stress does not change significantly in this initial phase (between A and B). With a delayed onset the (542) facets are formed. During their development and the further delayed onset of the formation of the (321) facets the intrinsic stress is significantly lowered (between B and C). The next two facet types, (532) and (954), grow simultaneously. Their stress contributions turn the stress change into the tensile direction, counteracting the previously compressive tendency (between C and D).

At coverages between 0.4 and 0.6 ML, the surface stress changes only slightly. In this coverage regime (between D and E), the population of the (111) terraces by PTCDA molecules begins (figure 3). At a coverage of 0.6 ML, the new facet type (743) is formed at the expense of the (321), (532), and (954) facets. This final morphology transition causes a further reduction of surface stress, which is not finished after all material has been adsorbed. Equilibrium of both, stress and morphology, is finally reached after approximately 20 min of annealing.

The results of these measurements have important and unexpected consequences. First of all, the magnitude of the total stress change upon PTCDA deposition is on both surfaces, Ag(10 8 7) and Ag(111), significantly larger than those previously measured in systems involving organic adsorbates (e.g. -0.1 N m^{-1} for pentacene/Si(111) [37], or -0.08 to -0.19 N m^{-1} for various alkanethiols on Au(111) [38]). At least two mechanisms contribute to the measured compressive net changes of surface stress. On both surfaces the local charge transfer from the silver substrate into the lowest unoccupied molecular orbital of the adsorbate [27, 31] reduces the

intrinsic tensile surface stress of the first atomic substrate layers [30]. The larger value for the faceted interface can be explained by considering that the originally equidistant mono-atomic steps are bunched together in the faceting process, overcoming their mutual repulsive step interaction, and by the stronger chemisorptive bond of PTCDA on vicinal surfaces as compared to (111). Thus, additional compressive stress is built up.

Furthermore, the clear correlation between changes of morphology and structure on the one hand and surface stress on the other hand indicates that the formation of specific facet types is determined by their stress contribution. In particular, the observation that facets inducing tensile and compressive surface stress changes appear subsequently is fundamental for the understanding of the kinetics of faceting processes. It appears reasonable that the formation of the (532) and (954) facets in section C–D reduces the stress generated by the initial (321) facet formation. This finding strongly suggests that the system tries to limit the net stress change by creating new facets. A balanced net surface stress is thus found to be a decisive driving force for the large-scale reconstruction of the surface. This effect must be compared with other, perhaps more obvious boundary conditions determining the kinetics of the faceting process. Such alternative conditions are, e.g., the preferred formation of defect-free boundary lines between adsorbate domains, a maximum gain in adsorption energy, and the inevitable conservation of the average macroscopic orientation.

Finally, our assignment of different stress regimes to morphological objects of mesoscopic dimensions (i.e. the facets) is equivalent to the identification of so-called [39, 40] stress domains on the surface. These domains lead to stress discontinuities and induce effective force monopoles at the domain boundaries. In the Marchenko-Alerhand model [39, 40], the existence of these force monopoles promotes the equidistant spacing of domains with critical sizes. Thus, our experimental data provide clear evidence that it is indeed surface stress which plays a decisive role for the ordering on the mesoscale. Notably, the observed magnitude of the net stress differs only by a factor of 2 from that measured in the Cu–CuO system [41–43]. Therefore, the strength of the elastic interaction appears to be large enough for this system, and, more importantly, hence also for the entire system class to enable the observed self-organized long-range ordering.

We emphasize that the data give experimental evidence that surface stress is a decisive quantity and driving force not only for the formation of surface reconstructions [29, 30, 44], but also of faceting. It supports theoretical models based on elasticity [39, 40] to explain the long-range order of these systems in equilibrium. Nevertheless, a refined theoretical description seems desirable to understand finer details inherent to periodically faceted systems, like multiple domain species, rules for their actual selection, and order of their appearance. Moreover, a comparison of the bonding strengths of PTCDA on the various facets provided by sophisticated density functional calculations would be of great value to better understand the selection of facets and hence the driving forces behind the reconstruction behavior. Of course, such calculations would be very challenging and at the forefront of present facilities because the required unit cells are very large and the differences between different bonding configurations might be small.

In conclusion, the change of surface stress during faceting of a metal surface induced by adsorption of an organic molecule has been measured for the first time. Moreover, the evolution of surface stress as function of molecular coverage has been correlated with large morphological transitions in the adsorbate system utilizing *in situ* LEEM and SPA-LEED measurements. This experimental combination quantifies the correlation between surface stress and faceting and allows ascribing stress changes to the appearance of specific facets. Thus, the present results reveal the elastic contribution to long-range self-organization and present experimental evidence supporting corresponding theoretical descriptions.

Acknowledgments

The authors would like to thank M Lukacs and H Menge for preparing the substrates, and C Kumpf for fruitful discussions. One of us (EU) appreciates financial support by the Fonds der Chemischen Industrie.

Author contributions

SS: performed the STM experiments. FP performed all other experiments and the data analysis. PV, ZT, and DS were involved in the cantilever experiments. CS participated in the SPA-LEED measurements. FM, HM, and TS carried out the LEEM experiments. The experiments, data analysis, and the manuscript were intensively discussed by FP, DS, AS, SS, TS, JK, and EU. The paper was written by FP, DS, AS and EU.

References

[1] Oura K, Lifshits V, Saranin A, Zotov A and Katayama M 2003 (Berlin: Springer)
[2] Abadía M, González Moreno R, Sarasola A, Otero Irurueta G, Verdini A, Floreano L, Garcia Lekue A and Rogero C 2014 *J. Phys. Chem.* C **118** 29704
[3] Maughan B, Zahl P, Sutter P and Monti O L 2015 *J. Phys. Chem.* C **119** 27416
[4] Xiao W, Ruffieux P, Aït Mansour K, Gröning O, Palotas K, Hofer W A, Gröning P and Fasel R 2006 *J. Phys. Chem.* B **110** 21394

[5] Gavioli L, Fanetti M, Sancrotti M and Betti M G 2005 *Phys. Rev.* B **72** 035458
[6] Barth J V, Costantini G and Kern K 2005 *Nature* **437** 671
[7] Nötzel R, Niu Z, Ramsteiner M, Schönherr H P, Tranpert A, Däweritz L and Ploog K H 1998 *Nature* **392** 56
[8] De Oteyza D, Krauss T, Barrena E, Sellner S, Dosch H and Osso J 2007 *Appl. Phys. Lett.* **90** 243104
[9] Heringdorf F J M Z, Kähler D, Horn von Hoegen M, Schmidt T, Bauer E, Copel M and Minoda H 1998 *Surf. Rev. Lett.* **5** 1167
[10] Zu Heringdorf F J M, Schmidt T, Heun S, Hild R, Zahl P, Ressel B, Bauer E and Horn von Hoegen M 2001 *Phys. Rev. Lett.* **86** 5088
[11] Zach M P, Ng K H and Penner R M 2000 *Science* **290** 2120
[12] Ma X, Meyerheim H, Barthel J, Kirschner J, Schmitt S and Umbach E 2004 *Appl. Phys. Lett.* **84** 4038
[13] Jensen H, Berndt R, Rurali R and Lorente N 2006 *J. Phys. Condens. Matter* **18** S51
[14] Brovko O O, Bazhanov D I, Meyerheim H L, Sander D, Stepanyuk V S and Kirschner J 2014 *Surf. Sci. Rep.* **69** 159
[15] Shen Z, Burrows P E, Bulović V, Forrest S R and Thompson M E 1997 *Science* **276** 2009
[16] Jakabovic J *et al* 2013 *Synth. Met.* **175** 47
[17] Agrawal R, Kumar P and Ghosh S 2008 *IEEE Trans. Electron Devices* **55** 2795
[18] Eremtchenko M, Schaefer J A and Tautz F S 2003 *Nature* **425** 602
[19] Tautz F 2007 *Prog. Surf. Sci.* **82** 479
[20] Glöckler K, Seidel C, Soukopp A, Sokolowski M, Umbach E, Böhringer M, Berndt R and Schneider W D 1998 *Surf. Sci.* **405** 1
[21] Kilian L, Umbach E and Sokolowski M 2004 *Surf. Sci.* **573** 359
[22] Chkoda L, Schneider M, Shklover V, Kilian L, Sokolowski M, Heske C and Umbach E 2003 *Chem. Phys. Lett.* **371** 548
[23] Marchetto H, Schmidt T, Groh U, Maier F C, Lévesque P L, Fink R H, Freund H J and Umbach E 2015 *Phys. Chem. Chem. Phys.* **17** 29150
[24] Krause B, Dürr A, Schreiber F, Dosch H and Seeck O 2004 *Surf. Sci.* **572** 385
[25] Schmitt S, Schöll A and Umbach E 2016 *Surf. Sci.* **643** 59
[26] Schmitt S 2007 *PhD Thesis* Würzburg
[27] Zou Y, Kilian L, Schöll A, Schmidt T, Fink R and Umbach E 2006 *Surf. Sci.* **600** 1240
[28] Ikonomov J, Bauer O and Sokolowski M 2008 *Surf. Sci.* **602** 2061
[29] Sander D and Kirschner J 2007 *Appl. Phys.* A **87** 419
[30] Ibach H 1997 *Surf. Sci. Rep.* **29** 195
[31] Ziroff J, Forster F, Scholl A, Puschnig P and Reinert F 2010 *Phys. Rev. Lett.* **104**
[32] Bauer E 1998 *Surf. Rev. Lett.* **05** 1275
[33] Levesque P, Marchetto H, Schmidt T, Maier F C, Freund H J and Umbach E 2016 *J. Phys. Chem.* C **120** 19271
[34] Marchetto H, Groh U, Schmidt T, Fink R, Freund H J and Umbach E 2006 *Chem. Phys.* **325** 178
[35] Scheithauer U, Meyer G and Henzler M 1986 *Surf. Sci.* **178** 441
[36] Horn von Hoegen M 1999 *Z. Kristallogr.* **214** 591
[37] Kury P, Roos K R, Horn von Hoegen M and Heringdorf F J M Z 2008 *New J. Phys.* **10** 023037
[38] Berger R, Delamarche E, Lang H P, Gerber C, Gimzewski J K, Meyer E and Güntherodt H J 1997 *Science* **276** 2021
[39] Alerhand O L, Vanderbilt D, Meade R D and Joannopoulos J D 1988 *Phys. Rev. Lett.* **61** 1973
[40] Marchenko V 1981 *Sov. Phys. JETP* **54** 605
[41] Bombis C, Moiseeva M and Ibach H 2005 *Phys. Rev.* B **72** 245408
[42] Prévot G, Croset B, Girard Y, Coati A, Garreau Y, Hohage M, Sun L and Zeppenfeld P 2004 *Surf. Sci.* **549** 52
[43] Harrison M, Woodruff D, Robinson J, Sander D, Pan W and Kirschner J 2006 *Phys. Rev.* B **74** 165402
[44] Bach C E, Giesen M, Ibach H and Einstein T L 1997 *Phys. Rev. Lett.* **78** 4225